



1 **Tracing subducted oceanic slabs in the mantle by**
2 **using molybdenum isotopes: A case study of**
3 **intraplate basalts from the Northeast China**

4
5 Qiugen Zheng^A, Qifang Zheng^{B*}, Yi Zhang^{C*}, Guangyu He^D, Qian Wang^D, Jane Fitton^E

6 A.School of Ocean Sciences, China University of Geosciences (Beijing), Beijing,
7 China,100083

8 B. School of Earth Sciences and Resources, China University of Geosciences (Beijing),
9 Beijing, China,100083

10 C.School of Earth Sciences, ZheJiang University, Hangzhou, China, 310058

11 D. State Key Laboratory of Isotope Geochemistry, Guangzhou Institute of Geochemistry,
12 Chinese Academy of Sciences, Guangzhou, China, 510630

13 E. Dept of Earth Sciences, University of Oxford, South Parks Road, Oxford OX1 3AN, UK

14

15

16 * Corresponding author:

17 Qifang Zheng and Yi Zhang

18 E-mail: xiaoyi_tu2021@163.com

19 zhangyi920407@163.com

20

21

22



23 **Abstract**

24 Determining subducted processes is very important for understanding lithological
25 heterogeneity because substantial quantities of slabs are recycled into the mantle. Molybdenum
26 isotopes have been used to distinguish sources materials because of the significant Mo isotopic
27 differences between the crust and the mantle. Here, we undertake a systematic Mo isotopic
28 investigation on a suite of well-characterized continental basalts from Keluo and Halaha-
29 Chaoer, located in Northeast China. $\delta^{98}\text{Mo}$ of Keluo varied from -0.41 to -0.23‰ with an
30 average of -0.34‰, and samples from Halaha-Chaoer ranged in $\delta^{98}\text{Mo}$ from -0.18 to -0.12‰
31 with an average of -0.15‰. The former is lighter than the mean value of fresh oceanic basalts
32 (-0.21‰), while the latter is similar to oceanic basalts. Combined with other geochemical
33 indications (LOI, Ce/Pb, La/Yb and so on), the Mo isotopic variations cannot be interrupted by
34 chemical weathering, continental crust contamination, or magmatic processes. The $\delta^{98}\text{Mo}$
35 variation in this study is explained by adding various oceanic crustal materials in magma
36 sources. The relationships of $\delta^{98}\text{Mo}$ with Ba/Th, Th/U, $^{143}\text{Nd}/^{144}\text{Nd}$ for the samples indicated
37 that sediment and altered oceanic crust have contributed to the significant variations in these
38 samples. This study indicates the great potential of Mo isotopes to distinguish different types
39 of recycled oceanic crust materials in the mantle.

40

41

42 Keywords: Molybdenum isotopes; Subducted oceanic slabs; Intraplate basalts; Northeast China

43



44 **1. Introduction**

45 Slab subduction is widely considered to be the primary mechanism for element cycling between
46 the crust and mantle (Hofmann, 1997; Stracke et al., 2003). The recycled materials with slabs
47 subduction are used to either generate the magmas in the subduction zone or form different
48 reservoirs, such as enriched mantle component I (EM I) and enriched mantle component II (EM
49 II) (Zindler and Hart, 1986). Previous investigations suggested that the oceanic crust account
50 for ~10% of the total mass of the mantle since the starting of subducted processes (Stracke et
51 al., 2003; Tang et al., 2016). The converted approach took varied materials into mantle and led
52 to lithological heterogeneity in the upper mantle (Perfit et al., 1980; Plank and Langmuir, 1998;
53 Castillo et al., 2000). Therefore, distinguishing the contribution of subducted materials was
54 required for understanding the lithological heterogeneity.

55 The previous works observed that the mobility of Mo could be negligible in the subduction
56 zones (Noll et al., 1996; Bali et al., 2012), suggesting that Mo isotopic composition of subduced
57 material can be recorded in the mantle (Freyduth et al., 2015). Supposing there are significant
58 differences in $\delta^{98}\text{Mo}$ and Mo concentration between the upper mantle, fresh oceanic crust,
59 altered oceanic crust, and sediment, the Mo isotope system will be a powerful tool to trace the
60 sources of magma and calculate the contribution proportion of each source. Bezdard et al. (2016)
61 measured the Mo isotopic composition of Mid-Ocean Ridges Basalt (MORB) to establish the
62 Mo isotopic composition of the depleted mantle (DM) as $-0.21 \pm 0.02\%$. Freyduth et al. (2015)
63 analyzed the sediment and altered oceanic crust from ODP sites 801 and 802, ranging in $\delta^{98}\text{Mo}$
64 from -1.87 to 0.11% with an average value of -0.50% and from -0.88 to 0.86% with an average
65 value of -0.03% , respectively. Moreover, the Mo concentrations of the upper mantle, altered
66 oceanic crust, and sediment are $1.65 \mu\text{g g}^{-1}$, $0.35 \mu\text{g g}^{-1}$, and $4.03 \mu\text{g g}^{-1}$, respectively. The
67 significant differences in Mo isotopic composition and Mo concentrations between mantle and
68 crust indicate that Mo isotope has excellent potential to trace subducted processes.

69 Due to the natural advantage of the Mo isotope, many investigations focused on oceanic basalt
70 using Mo isotopic system to trace the subducted processes (König et al., 2016; Willbold and
71 Elliott, 2017; Zhang et al., 2020; Li et al., 2021). However, the current Mo isotope data of
72 intraplate basalt is very limited, and it is debated for using Mo isotope to trace recycled



73 materials for intraplate basalt. Here, we measured a systematic Mo isotopic composition of a
74 set of well-characterized basalt samples from Keluo and Halaha-Chaoer of Northeast China.
75 Samples from Keluo display typical EM I characteristics, while samples from Halaha-Chaoer
76 have the radiogenic isotopic signatures of the focal zone (FOZO) (Hart et al., 1992; Stracke et
77 al., 2005). Thus, the samples allow us to use the Mo isotope to assess the contributions of
78 recycled crustal materials to the mantle.

79 **2 Sample**

80 Northeast China was set between the Siberian Craton and the North China Craton, and
81 considered as the eastern segment of the Central Asian Orogenic Belt (Chen et al., 2007; Zhang
82 et al., 1995). The plate suffered the closure of the Paleo-Asian Ocean and the amalgamation of
83 many microcontinent (Senger et al., 1993). Intraplate basaltic rocks in North China were formed
84 in the Cenozoic (Zhang et al., 1995; Zou et al., 2003). The Halaha-Chaoer and Keluo volcanic
85 fields were set at the Great Xing'an Mountains and the North of Songliao Basin (Zhang, 1992).
86 Fourteen samples were collected from two volcanic fields, including Halaha-Chaoer (2.0 Ma)
87 and Keluo (9.6–0.11 Ma), of Northeast China. These samples come from many works which
88 studied the evolution of volcanoes. Therefore, the geochemical and isotopic compositions of
89 more samples can be found in previous works (Sun et al., 2014, 2017), and particle samples are
90 measured in this study (Table S1). Here, we just provided a brief description of these samples.
91 The Mo concentration and MgO content of Halaha-Chaoer lavas ranged from 0.96 to 1.18 μg
92 g^{-1} with an average value of $1.05 \pm 0.18 \mu\text{g g}^{-1}$ and from 7.93 to 12.13 wt. %, suggesting
93 significant crystallization. And the Sr-Nd isotopic ratios of Halaha-Chaoer samples is similar
94 to the FOZO component (initial $^{87}\text{Sr}/^{86}\text{Sr} = 0.70354 - 0.7037$ and $^{143}\text{Nd}/^{144}\text{Nd} = 0.51291 -$
95 0.5193). On the contrary, the Keluo lavas are characterized by a high Mo concentration of 1.21-
96 $2.63 \mu\text{g g}^{-1}$ and same MgO content (7.67 to 11.28 wt.%) in relation to Halaha-Chaoer lavas. The
97 Sr-Nd isotopic compositions of the group sample are close to the EMI component ($^{87}\text{Sr}/^{86}\text{Sr} =$
98 $0.70503-0.70541$ and $^{143}\text{Nd}/^{144}\text{Nd} = 0.51235-0.51246$) (Table 1). The significant chemical
99 difference between Keluo and Halaha-Chaoer provided a great opportunity to check the ability
100 of Mo isotope to trace the contributions of recycled crustal materials to the mantle.

101 **3 Analytical methods**



102 3.1 Major and trace element analyses

103 The major and trace elements were conducted following the analytical procedures described by
104 Qi et al. (2000). An Inductively Coupled Plasma-Atomic Emission Spectrometer measured the
105 major elemental compositions. The loess on ignition (LOI) was analyzed after the samples were
106 heated for 30 min at 980°C. The samples were digested using a mixture of HF-HNO₃-HF. The
107 clean solutions were diluted to determine the trace element composition on an Inductively
108 Coupled Plasma-Mass Spectrometry (ELEMENT XR, Thermo, Germany). The reproducibility
109 for trace elements is better than 10% (2SD). All uncertainties of the major element are better
110 than 2% (2SE).

111 3.3 Mo-Sr-Nd isotopic analyses

112 The Mo isotopic measurement of all samples was carried out at the State Key Laboratory of
113 Isotope Geochemistry, Guangzhou Institute of Geochemistry, Chinese Academy of Sciences.
114 Detailed processes for digestion, chemical purification and isotopic analysis can be found in Li
115 et al. (2014) and Zhao et al. (2017). Sr-Nd isotopes were determined at the China University of
116 Geosciences, Beijing, and a more analyzed method can be found in Xu et al. (2021).

117 The samples were digested using a 7 ml PFA beaker. Approximately 50-100 mg of powdered
118 samples were mixed with 2ml of concentrated HF and 1 ml of concentrated HNO₃; the mixtures
119 were heated at 185±5°C for 36 h. The dry residues were dissolved into Aqua regia to digest
120 samples completely. The fully dissolved samples were evaporated to dryness and then
121 redissolved in 5ml 1.5 M HNO₃.

122 The digested samples containing 100-200 ng Mo were spiked by the double spikes (¹⁰⁰Mo-⁹⁷Mo)
123 in a 15ml PFA beaker to correct the potential Mo isotopic fractionation of chemical purification
124 and measurement. The spiked samples were dried slowly at 90°C to allow the equilibration
125 between the samples and double spike and then redissolved in 4ml mixed acid of 0.1 M HF and
126 1M HCl. The sample solutions were loaded to prepare BPHA resin that was clean with 6 M
127 HCl and MQ. The matrix elements were washed out of columns by 0.1M HF-1M HCl. The
128 fraction of Mo was collected by 6 M HF-1M HCl in a 15ml PFA beaker. The eluted solutions
129 were evaporated to dry at 130°C. Concentrated HNO₃ and H₂O₂ were used to remove residual
130 organic materials from the resin. The total blank of the procedure is 0.5ng which can be



131 neglected in relation to the loaded sample. Sr and Nd were purified from matrix elements using
132 AG50W-X12 (200-400 mesh) resin and LN resin, respectively.

133 Molybdenum isotopic measurements were performed with a Multi-collector inductively
134 coupled plasma mass spectrometer (MC-ICP-MS, Neptune Plus, ThermoFisher). Sample
135 solutions were introduced into the plasma by an Aridus II desolvator system. The signal
136 sensitivity of ^{95}Mo was $\geq 190 \text{ V } \mu\text{g}^{-1} \text{ mL}$, and the blank signal of ^{95}Mo was less than 4 mV. The
137 solutions and samples were dissolved at 0.5 M HHNO_3 and diluted to 30 ng mL^{-1} for measuring
138 Mo isotopes. All Mo isotope analyses were carried out on the low mass resolution mode
139 ($\Delta\text{M}/\text{M} < 3000$). The on-peak instrument and acid matrix blank were determined by measuring
140 1.5M HNO_3 before each sample and standard to subtract from the signal intensities. Every 5
141 samples were bracketed by a spiked SRM 3134 with 30 ng mL^{-1} to normalize the Mo isotope
142 ratio of samples. More detailed parameters for the Mo isotopes measurements have been listed
143 in previous work. The Mo isotopic composition is expressed relative to NIST SRM 3134 as
144 delta (δ) notation: $\delta^{98}\text{Mo} = \left(\frac{^{98}\text{Mo}/^{95}\text{Mo}}{(^{98}\text{Mo}/^{95}\text{Mo})_{\text{NIST SRM 3134-1}}} - 1 \right) \times 1000$. Four
145 geological reference materials (NOD-A-1, NOD-P-1, BHVO-2 and BCR-2) from USGS were
146 digested, purified and measured with our samples. The Mo isotopic compositions re $-0.79 \pm 0.04\%$
147 (2SD, n=5) for NOD-A-1, $-0.87 \pm 0.05\%$ (2SD, n=5) for NOD-P-1, $-0.05 \pm 0.05\%$ (2SD, n=5)
148 for BHVO-2 and $-0.06 \pm 0.04\%$ (2SD, n=5) for BCR-2, similar to previous works (Skierszkan
149 et al., 2015; Li et al., 2016; Willbold et al., 2016).

150 For Sr and Nd isotopic composition, the mass fractionations of chemical purification and
151 instrument were calibrated with $^{88}\text{Sr}/^{86}\text{Sr} = 8.375209$ and $^{146}\text{Nd}/^{144}\text{Nd} = 0.7219$. The long-term
152 analysis gave 0.710241 ± 24 for $^{87}\text{Sr}/^{86}\text{Sr}$ of NIST SRM 987 in the lab and 0.512434 ± 29 for
153 $^{143}\text{Nd}/^{144}\text{Nd}$ of Alfa Aesar Nd. The Sr and Nd isotopic composition of BHVO-2 and BCR-2
154 determined in this study are consistent with previous values (Li et al., 2012).

155 **4. Results**

156 The $\delta^{95}\text{Mo}$ values of Northeast China lavas vary from -0.41% to -0.12% (Table 1). The sample
157 from Keluo varied from -0.41 to -0.23% in $\delta^{95}\text{Mo}$ with an average of $-0.34 \pm 0.10\%$ (2SD),
158 higher than the sediments (-0.50%) and lighter than the altered oceanic basalts (0.03%)
159 (Freyruth et al., 2015). The samples from Halaha-chaoer have homogenous Mo isotopic



160 composition, ranging from -0.12 to -0.18‰ with an average of -0.15 ± 0.05 ‰ (2SD), similar to
161 the fresh MORB (-0.21‰, Chen et al., 2022). The Sr-Nd isotopes, major and trace elements
162 composition were shown in Table 1 and Table S1.

163 **5. Discussion**

164 Given Mo isotope can be fractionated during a range of processes, it is necessary to carefully
165 assess the processes that may have modified Mo isotopic composition of these samples, such
166 as chemical weathering, assimilation of shallow continental crust, magmatic differentiation and
167 partial melting. And then, we estimate the effects of recycled crustal materials on the Mo
168 isotopic variation of the samples.

169 **5.1 Chemical weathering and Assimilation of crustal materials on Mo isotope**

170 Mo isotopes were fractionated during chemical weathering, and lighter isotopes adsorbed onto
171 secondary minerals so that the weathered residual is lighter in $\delta^{95}\text{Mo}$ than fresh igneous rocks
172 (Greaney et al., 2021). However, the samples do not observe secondary minerals (Sun et al.,
173 2014). Moreover, the loss on ignition (LOI) ranging from 0.00 to 1.28 does not display a
174 negative correlation (Fig. 1). Both pieces of evidences imply that the observed Mo isotopic
175 variation cannot be attributed to chemical weathering.

176 These basalts erupted through the continental crust, which is about 40km. The Mo content of
177 these basalts varies from 1.28 to 2.82 $\mu\text{g g}^{-1}$ with an average value of 1.83 $\mu\text{g g}^{-1}$, higher than
178 the average Mo concentration of continental crust is 0.8 $\mu\text{g g}^{-1}$ (Rudnick and Gao, 2014). The
179 upper continental crust is significantly different in $\delta^{95}\text{Mo}$ from the basalt (Yang et al., 2017;
180 Greaney et al., 2020). Hence, we must consider that crustal materials may modify the Mo
181 isotopic composition of these basalts. For the scenario, a negative correlation between Mo
182 content and $\delta^{95}\text{Mo}$ were expected because of the heavy Mo isotopic composition of the
183 continental crust. However, we do not observe the relationship (Fig. 2). On the other hand,
184 binary mixing calculation implies that the Mo isotopic variation cannot be explain by binary
185 mixing between continental crust and mantle melt, because of unrealistic Mo concentration
186 ratio (Fig. 2). Hence, Assimilation of crustal materials is not the main process that led to the
187 Mo isotopic variation in these basalts.

188



189 **5.2 The effect of fractional crystallization on Mo isotope**

190 The Mo isotopic composition of basalts from the Kos Island arc system ranged from 0.3 to
191 0.6‰, indicating that Mo isotopes are fractionated during the fractional crystallization of
192 hornblende and biotite (Voegelin et al., 2014). However, Bezard et al. (2016) measured the Mo
193 isotopic composition of MORB from the Pacific-Antarctic ridge and the Mohns-Knipovich
194 ridge. The $\delta^{95}\text{Mo}$ did not show correlations with MgO that indicated magma differentiation,
195 suggesting that Mo isotopic fractionation is insignificant during the fractional crystallization of
196 MORB magma. Recently, Chen et al. (2022) analyzed some MORB glass to constrain the Mo
197 isotopic composition of the upper mantle. The correlations between $\delta^{95}\text{Mo}$ and magmatic
198 differentiation indicators were not observed, inferring that Mo isotopes were not fractionated
199 during magmatic differentiation (Chen et al., 2022). For our samples studied here, the
200 significant variation of MgO contents (from 6.9 to 13.0%) implies that fractional crystallization
201 plays an essential role in changing the chemical composition of basalts. As shown in Fig.3a,
202 Mo concentration in basalt from Northeast China correlates well with MgO; the positive
203 correlation indicates that Mo is a likely incompatible element enriched in solid phases during
204 melt evolution. The unclear correlations between $\delta^{98}\text{Mo}$ and MgO (Fig. 3b) and Mo (Fig. 2)
205 content suggest that the effect of fractional crystallization on the $\delta^{95}\text{Mo}$ of basalts is likely
206 insignificant. The observation is similar to the previous inference (Bezard et al., 2016 and Chen
207 et al., 2022) but different from the conclusions from Voegelin et al. (2014). Thus, the $\delta^{98}\text{Mo}$
208 variation cannot be explained simply to fractional crystallization and may be caused by partial
209 melting.

210 **5.3 The effect of partial melting on Mo isotopic composition of basalts**

211 Since sodium is a moderately incompatible element at melting the with highest concentration
212 at started melting, the Na concentration of melt decreases with the growth of melting degree.
213 Hence, $\text{Na}_{8,0}$ indicates the degree of partial melting without the effect of fractional
214 crystallization (Klein and Langmuir, 1987). Bezard et al. (2016) observed the absence of
215 correlation between $\delta^{95}\text{Mo}$ and $\text{Na}_{8,0}$, explaining the trend that Mo isotopes are not fractionated
216 during mantle melting. Since La is more incompatible than the heavy rare earth element Yb
217 during the partial melting of mantle, $(\text{La}/\text{Yb})_N$ ratio is sensitive to the degree of partial melting.



218 Liang et al. (2017) observe broad correlations between $\delta^{98}\text{Mo}$ and $(\text{La}/\text{Yb})_{\text{N}}$ in ocean island
219 basalts (OIB), suggesting a significant effect of melting on the Mo isotopic variations. The
220 conclusion is contrary to Bezar et al. (2016). However, for our samples, we did not observe
221 the clear relationships between $\delta^{98}\text{Mo}$ and $\text{Na}_{8.0}$ (Fig. 4a) as well as $(\text{La}/\text{Yb})_{\text{N}}$ (Fig. 4b). In
222 addition, McCoy-West et al. (2019) accessed the Mo isotopic behaviors using a non-modal
223 batch melting model and inferred that Mo isotopes were significantly fractionated during
224 mantle partial melting that melt is heavier in $\delta^{98}\text{Mo}$ than the residue. The fractionation was
225 driven from as that Mo (VI) with heavier isotope is more incompatible than Mo (IV) (Leitzke
226 et al., 2017). However, the samples ($-0.33\pm 0.10\%$) produced by the high degree of partial
227 melting have lighter Mo isotopic composition than the samples with a low degree ($-$
228 $0.15\pm 0.05\%$), contrary to the prediction trend by the previous model (Fig. 4, McCoy-West et
229 al., 2019). Therefore, the evidences suggested that partial melting cannot explain the $\delta^{98}\text{Mo}$
230 variation of these basalts.

231 **5.4 Molybdenum isotopic variation induced by crustal recycling**

232 The above discussions show that the Mo isotopic variation for these basalts cannot be explained
233 by shallow-level processes, fractional crystallization and partial melting. Radiogenic isotopes,
234 such as Nd and Sr, usually are used to reflect heterogeneous sources. The significant variations
235 for $^{143}\text{Nd}/^{144}\text{Nd}$ and $\delta^{98}\text{Mo}$ imply that there are more than two components at least for the mantle
236 sources of these basalts (Fig. 5). In the following, we will discuss the mechanisms that may be
237 responsible for the processes of mantle enrichment and abnormal Mo isotopic composition.

238

239 Sediments could be recycled into the mantle with subducted slabs (Stracke et al., 2003). The
240 $\delta^{98}\text{Mo}$ of subducting sediments varied from -1.87 to 0.11% with an average value of $-0.50 \pm$
241 0.27% (2SE, $n=16$, Freymuth et al., 2015). Since Mo is a highly incompatible element and
242 lighter isotopes were preserved in the residual produced during metamorphic dehydration
243 (König et al., 2016), melts derived from recycled sediments should inherit the light Mo isotopic
244 composition. Hence, the incorporation of recycled sediments into peridotite melting could be
245 responsible the lighter Mo isotopic composition. The $\delta^{98}\text{Mo}$ of basalt studied here (-0.30%) is
246 lighter than fresh MORB (-0.21% , Chen et al., 2022), and $^{143}\text{Nd}/^{144}\text{Nd}$ is higher than sediment



247 (0.51228, Vervoort et al., 2011) and lighter than fresh MORB (0.513074, Gale et al., 2013),
248 suggesting that sediment is one of source for these basalts from Keluo. On the other hand, Th/U
249 ratio is not fractionated significantly during magmatic processes as Th and U are incompatible
250 elements. Both elements can be fractionated during fluid processes because of the higher
251 mobility of U than Th (Hawkesworth et al., 1997; Bali et al., 2009; Ling et al., 2011). Thus,
252 there is a significant difference in the Th/U ratio between fresh MORB (3.54, Gale et al., 2013)
253 and sediment (6.64, Vervoort et al., 2011). Reasonably, the ratio is usually used as an indicator
254 of distinguishing the mantle sources (Sun et al., 2020). The Th/U ratio of our basalts (4.94 to
255 6.12) falls between sediment and fresh MORB. The observation indicates that sediment may
256 play an essential role in forming these basalts. It is noteworthy that there is not expected positive
257 correlation between $\delta^{98}\text{Mo}$ and Th/U ratio (Fig. 5b), implying other sources for the basalts.
258 Significant Mo isotopic fractionation is observed during seawater alteration (Freyduth et al.,
259 2015), suggesting that altered oceanic crust (-0.02‰) is heavier $\delta^{98}\text{Mo}$ than fresh ocean crust
260 (-0.21‰). Thus, The incorporation of altered oceanic crust during the particle melting of mantle
261 could produce melts with significant various Mo isotopic composition. Due to the mobility
262 difference between Ba and Th (Weaver et al., 1986), the Ba/Th ratio of the altered oceanic crust
263 will be increased with the growing extent of low-temperature hydrothermal alteration (Kelley
264 et al., 2003). Furthermore, the ratio will not be changed during slab dehydration (Kogiso et al.,
265 1997; Kessel et al., 2005). Hence, the ratio is used to trace the incorporation of altered oceanic
266 crust in the mantle (Sun et al., 2020). The Ba/Th ratios of these basalts range from 147 to 239,
267 higher than sediment and fresh MORB and similar to altered oceanic crust (Fig. 5c), indicating
268 the incorporation of altered oceanic crust into the source region of these basalts.
269 Therefore, recycled sediment and altered both have contributed to the basalt of Keluo produced
270 in Northeast China. The materials may have come from the westward subduction of the Pacific
271 plate (Tang et al., 2014). The contribution of the fresh oceanic crust is insignificant because of
272 the low Mo concentration. Mixing of melts produced from recycled sediment with the
273 contribution of mantle peridotites derived the variation of Mo isotopic composition in the
274 basalts.

275 **6. Conclusion**



276 This work suggests that the basalt from Keluo displays heterogenous Mo isotopic composition
277 and is heavier Mo isotopic compositions than the upper mantle. At the same time, the sample
278 from Halaha-Chaoer is homogenous in $\delta^{98}\text{Mo}$, similar to the upper mantle. The isotopic
279 variation was explained by adding sediment and altered oceanic basalt with subducted oceanic
280 slabs into mantle sources. Therefore, the Mo isotope is a powerful tool in investigating the
281 effect of crustal recycling on mantle-derived magmas to understand recycling materials' roles
282 in mantle heterogeneity.

283

284 **Acknowledgements**

285 We are grateful to Jie Li and FanHuang Li for analytical assistance, as well as Yang Sun and
286 Yongwei Zhao for sample collection. The work was supported by the National Key Research
287 and Development Program of China (2017YFC0703201), the National Science and Technology
288 Major Project of the Ministry of Science and Technology of China (2016ZX05014001), the
289 Strategic Priority Research Program of the Chinese Academy of Sciences (XDA14010201), the
290 National Natural Science Foundation of China (41530347, 41872225)

291 **Reference**

- 292 Bali E., Audetat A. and Keppler H. (2009) Mobility of U and Th in subduction zone fluids-A
293 synthetic fluid inclusion study. *Geochim. Cosmochim. Acta* 73(13), A80.
- 294 Bali, E., Keppler, H., Audetat, A., 2012. The mobility of W and Mo in subduction zone fluids and
295 the Mo–W–Th–U systematics of island arc magmas. *Earth Planet. Sci. Lett.* 351–352, 195–
296 207.
- 297 Bezard R., Fischer-Godde M., Hamelin C., Brennecka G. A. and Kleine T. (2016) The effects of
298 magmatic processes and crustal recycling on the molybdenum stable isotopic composition of
299 Mid-Ocean Ridge Basalts. *Earth Planet. Sci. Lett.* 453, 171–181.
- 300 C.J. Hawkesworth, S.P. Turner, F. McDermott, D.W. Peate, P. van Calsteren, U-Th isotopes in arc
301 magmas implications for element transfer from the subducted crust, *Science* 276 (1997) 551-
302 555.
- 303 Castillo P. R. (2015) The recycling of marine carbonates and sources of HIMU and FOZO ocean
304 island basalts. *Lithos* 216–217, 254–263.



- 305 Chen, S., Sun, P., Niu, Y., Guo, P., Elliott, T., Hin, R.C., 2022. Molybdenum isotope systematics of
306 lavas from the East Pacific Rise: constraints on the source of enriched mid-ocean ridge basalt.
307 Earth Planet. Sci. Lett. 578, 117283.
308 Commun. 12, 6015.
- 309 Freymuth H., Vils F., Willbold M., Taylor R. N. and Elliott T. (2015) Molybdenum mobility and
310 isotopic fractionation during subduction at the Mariana arc. Earth Planet. Sci. Lett. 432, 176–
311 186.
- 312 Gale A., Dalton C. A., Langmuir C. H., Su Y. and Schilling J.-G. (2013) The mean composition of
313 ocean ridge basalts. Geochem. Geophys. Geosyst. 14, 489–518.
- 314 Greaney, A.T., Rudnick, R.L., Romaniello, S.J., Johnson, A.C., Gaschnig, R.M., Anbar, A.D., 2020.
315 Molybdenum isotope fractionation in glacial diamictites tracks the onset of oxidative
316 weathering of the continental crust. Earth Planet. Sci. Lett. 534, 116083.
- 317 Hart S. R., Hauri E. H., Oschmann L. A. and Whitehead J. A. (1992) Mantle plumes and
318 entrainment-Isotopic evidence. Science 256, 517–520
- 319 Hofmann A. W. (1997) Mantle geochemistry: The message from oceanic volcanism. Nature 385,
320 219–229.
- 321 Kelley K. A., Plank T., Ludden J. and Staudigel H. (2003) Composition of altered oceanic crust at
322 ODP Sites 801 and 1149. Geochem. Geophys. Geosyst. 4, 8910. [https://doi.org/
323 10.1029/2002GC000435](https://doi.org/10.1029/2002GC000435)
- 324 Kessel R., Schmidt M. W., Ulmer P. and Pettko T. (2005) Trace element signature of subduction-
325 zone fluids, melts and supercritical liquids at 120–180 km depth. Nature 437, 724–727.
- 326 Klein E. and Langmuir C. H. (1987) Global correlations of ocean ridge basalt chemistry with axial
327 depth and crustal thickness. J. Geophys. Res. 92, 8089–8115
- 328 Kogiso T., Tatsumi Y. and Nakano S. (1997) Trace element transport during dehydration processes
329 in the subducted oceanic crust: 1. Experiments and implications for the origin of ocean island
330 basalts. Earth Planet. Sci. Lett. 148, 193–205.
- 331 König S., Wille M., Voegelin A. and Schoenberg R. (2016) Molybdenum isotope systematics in
332 subduction zones. Earth Planet. Sci. Lett. 447, 95–102.
- 333 Leitzke F. P., Fonseca R. O. C., Sprungb P., Mallmann G., Lagosa M., Michelya L. T. and Münker



- 334 C. (2017) Redox dependent behaviour of molybdenum during magmatic processes in the
335 terrestrial and lunar mantle: implications for the Mo/W of the bulk silicate Moon. *Earth Planet.*
336 *Sci. Lett.* 474, 503–515.
- 337 Li C.-F., Li X.-H., Li Q.-L., Guo J.-H., Li X.-H. and Yang Y.-H. (2012) Rapid and precise
338 determination of Sr and Nd isotopic ratios in geological samples from the same filament
339 loading by thermal ionization mass spectrometry employing a single-step separation scheme.
340 *Anal. Chim. Acta* 727, 54–60.
- 341 Li H. Y., Zhao R. P., Li J., Tamura Y., Spencer C., Stern R. J., Ryan J. G. and Xu Y. G. (2021)
342 Molybdenum isotopes unmask slab dehydration and melting beneath the Mariana arc. *Nat.*
343 *Arc). Lithos* 190–191, 440–448.
- 344 Li J., Liang X.R., Zhong L.F., Wang X.C., Ren Z.Y., Sun S.L., Zhang Z.F. and Xu J.F. (2014).
345 Measurement of the isotopic composition of molybdenum in geological samples by MC-ICP-
346 MS using a novel chromatographic extraction technique. *Geostand. Geoanal. Res.* 38, 345–
347 354,
- 348 Li, J., Liang, X.-R., Zhong, X.-C., Wang, Z.-Y., Ren, S.-L., Sun, Z.-F., Zhang, J.-F., Xu, J.-F., 2014.
349 Measurement of the isotopic composition of molybdenum in geological samples by MC-IC-
350 MS using a novel chromatographic extraction technique. *Geostand. Geoanal. Res.* 38 (3), 345–
351 354.
- 352 Liang Y. H., Halliday A. N., Siebert C., Fitton J. G., Burton K. W., Wang K. L. and Harvey J. (2017)
353 Molybdenum isotope fractionation in the mantle. *Geochim. Cosmochim. Acta* 199, 91–111.
- 354 Ling M. X., Wang F. Y., Ding X., Zhou J. B. and Sun W. D. (2011) Different origins of adakites
355 from the Dabie Mountains and the Lower Yangtze River Belt, eastern China: geochemical
356 constraints. *Int. Geol. Rev.* 53(5–6), 727–740.
- 357 McCoy-West A. J., Chowdhury P., Burton K. W., Sossi P., Nowell G. M., Fitton J. G., Kerr A. C.,
358 Cawood P. A. and Williams H. M. (2019) Extensive crustal extraction in Earth's early history
359 inferred from molybdenum isotopes. *Nat. Geosci.* 12, 946–951
- 360 Noll, P.D., Newsom, H.E., Leeman, W.P., Ryan, J.G., 1996. The role of hydrothermal fluids in the
361 production of subduction zone magmas: evidence from siderophile and chalcophile trace
362 elements and boron. *Geochim. Cosmochim. Acta* 60, 587–611.



- 363 Perfit, M., Gust, D., Bence, A., Arculus, R., Taylor, S.R., 1980. Chemical characteristics of island-
364 arc basalts – implications for mantle sources. *Chem. Geol.* 30 (3), 227–256.
- 365 Plank, T., Langmuir, C.H., 1998. The chemical composition of subducting sediment and its
366 consequences for the crust and mantle. *Chem. Geol.* 145, 325–394
- 367 Qi, L., Hu, J., Gregoire, D.C., 2000. Determination of trace elements in granites by inductively
368 coupled plasma–mass spectrometry. *Talanta* 51, 507–513.
- 369 Rudnick R. L. and Gao S. (2014) Composition of the continental crust. In *Treatise on Geochemistry*
370 (eds. H. D. Holland and K. K. Turekian), second ed. Elsevier, Oxford, pp. 1–51.
- 371 Skierszkan EK, Amini M, Weis D (2015) A practical guide for the design and implementation of the
372 double-spike technique for precise determination of molybdenum isotope compositions of
373 environmental samples. *Anal Bioanal Chem* 407:1925–1935
- 374 Stracke A., Bizimis M. and Salters V. J. M. (2003) Recycling oceanic crust: Quantitative constraints.
375 *Geochem. Geophys. Geosyst.* 4, 8003. <https://doi.org/10.1029/2001GC000223>, 3.
- 376 Stracke A., Hofmann A. W. and Hart S. R. (2005) FOZO, HIMU, and the rest of the mantle zoo.
377 *Geochem. Geophys. Geosyst.* 6, Q05007. <https://doi.org/10.1029/2004GC000824>.
- 378 Sun Y., Teng F.-Z., Ying J.-F., Su B.-X., Hu Y., Fan Q.-C. and Zhou X.-H. (2017) Magnesium
379 isotopic evidence for ancient subducted oceanic crust in LOMU-like potassium-rich volcanic
380 rocks. *J. Geophys. Res. Solid Earth* 122, 7562–7572.
- 381 Sun Y., Ying J., Zhou X., Shao J. A., Chu Z. and Su B. (2014) Geochemistry of ultrapotassic volcanic
382 rocks in Xiaogulihe NE China: implications for the role of ancient subducted sediments. *Lithos*
383 208–209, 53–66.
- 384 Tang Y., Obayashi M., Niu F., Grand S. P., Chen Y. J., Kawakatsu H., Tanaka S., Ning J. and Ni J.
385 F. (2014) Changbaishan volcanism in northeast China linked to subduction-induced mantle
386 upwelling. *Nat. Geosci.* 7, 470–475.
- 387 Vervoort J. D., Plank T. and Prytulak J. (2011) The Hf–Nd isotopic composition of marine sediments.
388 *Geochim. Cosmochim. Acta* 75, 5903–5926
- 389 Voegelin A. R., Pettke T., Greber N. D., von Niederhäusern B. and Nägler T. F. (2014) Magma
390 differentiation fractionates Mo isotope ratios: evidence from the Kos Plateau Tuff (Aegean
391 Willbold M. and Elliott T. (2017) Molybdenum isotope variations in magmatic rocks. *Chem. Geol.*



- 392 449, 253–268.
- 393 Willbold M., Hibbert K., Lai Y. J., Freymuth H., Hin R. C., Coath C., Vils F. and Elliott T. (2016)
- 394 High-precision mass-dependent molybdenum isotope variations in magmatic rocks determined
- 395 by double-spike MC-ICP-MS. *Geostand. Geoanal. Res.* 40, 389–403.
- 396 Xu L.-J., Liu S.-A. and Li S. (2021) Zinc isotopic behavior of mafic rocks during continental deep
- 397 subduction. *Geosci. Front.* 12(5) 101182.
- 398 Yang J., Barling J., Siebert C., Fietzke J., Stephens E. and Halliday A. N. (2017) The molybdenum
- 399 isotopic compositions of I-, S and A-type granitic suites. *Geochim. Cosmochim. Acta* 205,
- 400 168–186.
- 401 Zhang Y., Yuan C., Sun M., Li J., Long X., Jiang Y. and Huang Z. (2020) Molybdenum and boron
- 402 isotopic evidence for carbon recycling via carbonate dissolution in subduction zones. *Geochim.*
- 403 *Cosmochim. Acta* 278, 340–352.
- 404 Zhao, P.-P., Li J., Zhang L., Wang Z.-B., Kong D.-X., Ma J.-L., Wei G.-J., Xu J.-F.. (2015)
- 405 Molybdenum mass fractions and isotopic compositions of international geological reference
- 406 materials. *Geostand. Geoanal. Res.* 40, 217–226.
- 407 Zindler A. and Hart S. (1986) Chemical geodynamics. *Annu. Rev. Earth Planet. Sci.* 14, 493–571.
- 408



Table 1 Molybdenum isotopic composition of Northeast China basalt and geological reference materials

Sample	Mo($\mu\text{g g}^{-1}$)	MgO(%)	Na _{8.0}	LOI	Ce/Pb	Th/U	Ba/Th	(La/Yb) _N	⁸⁷ Sr/ ⁸⁶ Sr	¹⁴³ Nd/ ¹⁴⁴ Nd	$\delta^{98}\text{Mo}$	2SD
Keluo												
DYS12-01	2.42	7.93	3.61	0.86	10.9	4.94	239	40.6	0.70514	0.51240	-0.38	0.04
DYS12-02	2.45	7.89	3.48	0.75	9.83	5.01	224	43.7	0.70509	0.51241	-0.36	0.04
XYS12-01	2.63	8.02	4.12	0.16	8.53	5.06	147	47.7	0.70541	0.51239	-0.41	0.03
XYS12-04	2.53	8.6	3.98	0.4	17.0	5.15	176	49.1	0.70534	0.51236	-0.38	0.05
JS12-01	1.48	11.28	4.16	1.28	15.4	5.46	227	39.8	0.70511	0.51242	-0.32	0.04
JS12-02	1.52	11.3	4.25	0.9	15.2	5.40	223	36.3	0.70503	0.51243	-0.38	0.03
DZS12-02	1.46	11.43	4.90	0.08	17.6	5.52	202	41.5	0.70514	0.51243	-0.23	0.05
DZS12-03	1.32	11.62	5.09	0.06	17.0	4.93	231	44.3	0.70507	0.51246	-0.34	0.03
XGS12-01	1.73	10.11	4.04	0.68	9.26	4.96	201	42.8	0.70527	0.51238	-0.28	0.04
XGS12-02	1.88	9.93	4.02	0.34	9.99	5.87	198	43.2	0.70531	0.51238	-0.29	0.05
HS12-01	1.21	12.13	4.96	0.12	15.4	6.32	231	35.2	0.70514	0.51244	-0.34	0.04
HS12-03	1.38	12.05	5.02	0.06	20.35	6.12	238	37.2	0.70516	0.51241	-0.32	0.03
Halaha- Chaoer												
07CH02	1.04	12.97	4.64	0.10	17.40	4.13	134	10.2	0.70365	0.51293	-0.15	0.03
07AES07	1.01	10.88	4.27	0.30	12.14	4.09	105	10.3	0.70371	0.51291	-0.12	0.03
07AES09	0.96	10.43	4.13	0.12	15.59	3.98	97	9.4	0.70369	0.51293	-0.18	0.04
07AES16	1.18	12.5	4.82	0.11	20.34	4.44	109	9.9	0.70354	0.51293	-0.13	0.05
Geological reference materials												
NOD-P-1											-0.79	0.04
NOD-A-1											-0.87	0.05
BCR-2											-0.06	0.04
BHVO-2											-0.05	0.05

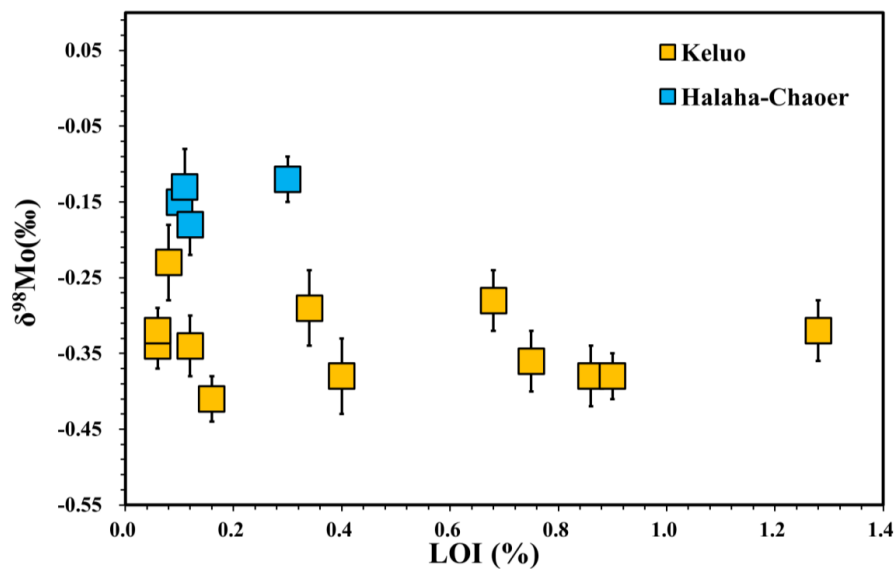


Fig.1 $\delta^{98}\text{Mo}$ versus loss on ignition (LOI) for Northeast China basalts. Data are reported in

Table 1

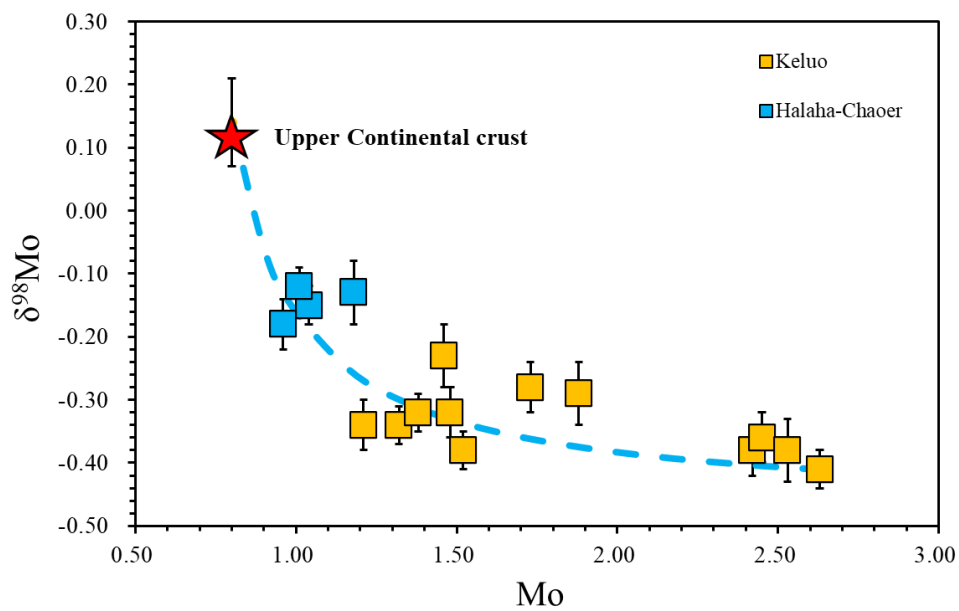


Fig.2 Plots of $\delta^{98}\text{Mo}$ against Mo concentration for Northeast China basalts. The average Mo isotopic composition of upper continental crust is $0.14 \pm 0.07\%$ (Yang et al., 2017). Data are reported in Table 1.

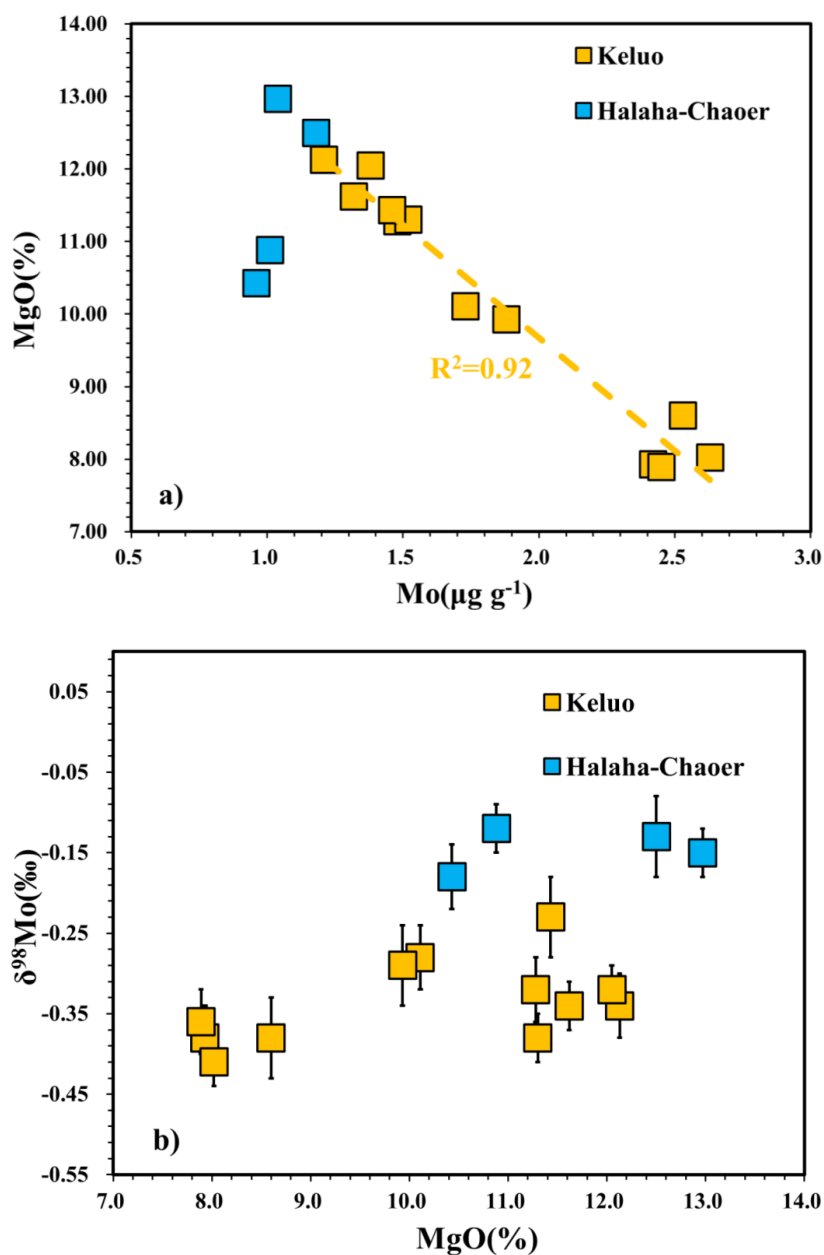


Fig. 3 Plot of $\delta^{98}\text{Mo}$ against Mo concentration (a) and MgO content (b) for Northeast China basalts.

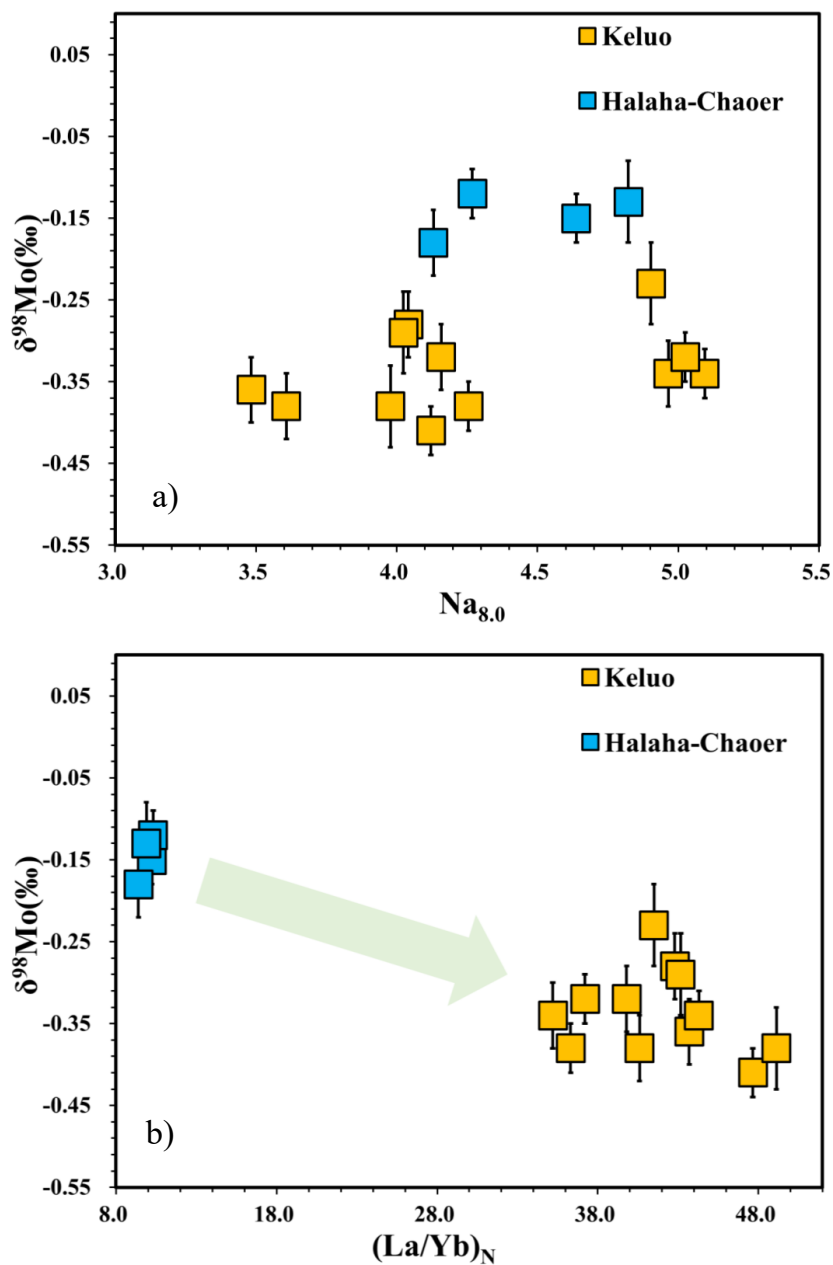
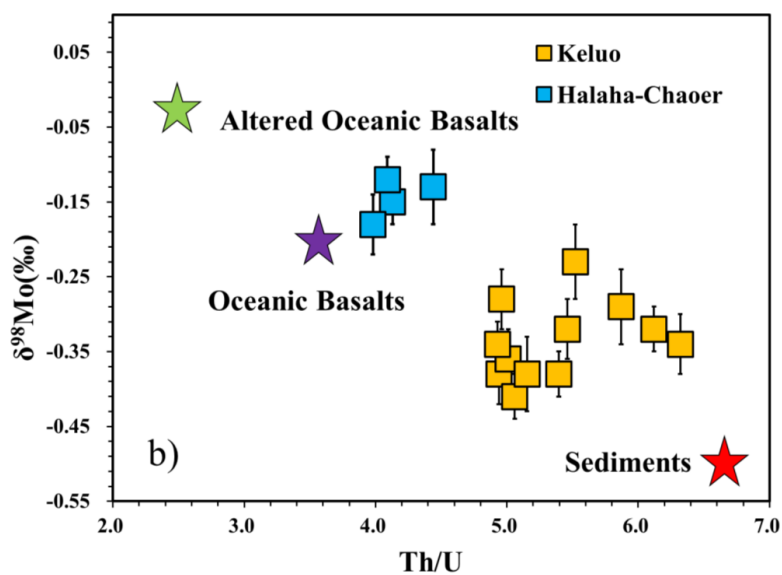
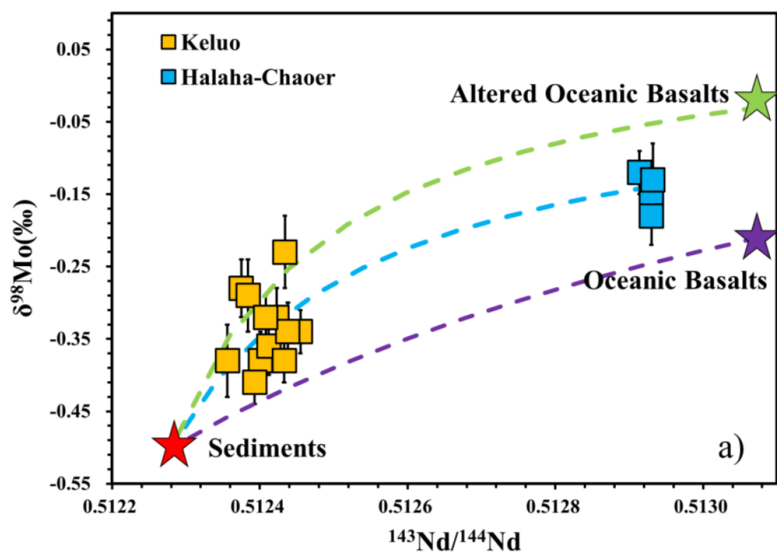


Fig. 4 $\delta^{98}\text{Mo}$ versus $\text{Na}_{8,0}$ (a) and $(\text{La}/\text{Yb})_N$ (b) for Northeast China basalts. $\text{Na}_{8,0}$ was calculated by $\text{Na}_{8,0} = \text{Na}_2\text{O} + (0.373 \times \text{MgO}) - 2.98$ (Klein and Langmuir, 1987). Data are reported in Table 1



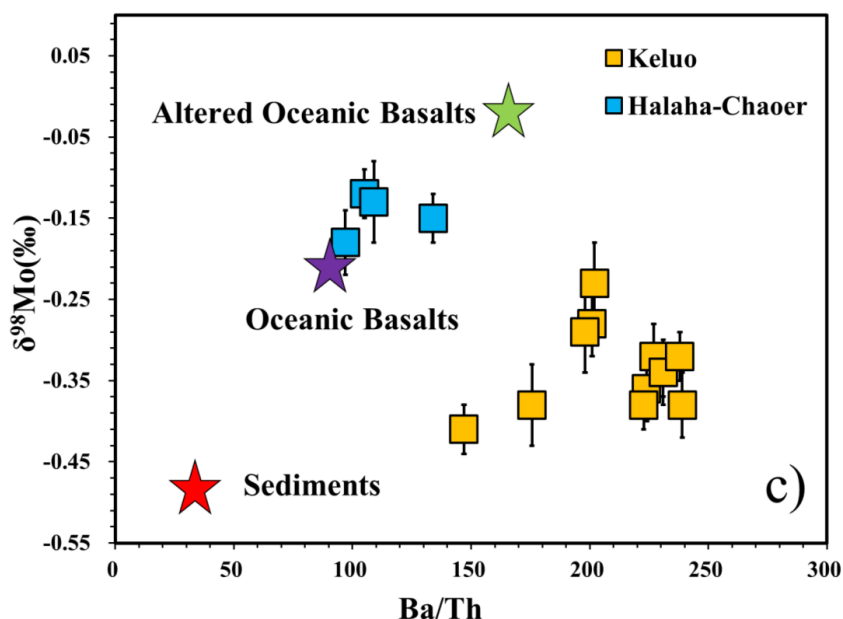


Fig. 5 Plot of $\delta^{98}\text{Mo}$ against $^{143}\text{Nd}/^{144}\text{Nd}$ (a), Th/U (b) and Ba/Th (C) for Northeast China basalts. The clay-rich sediments, highly altered oceanic crust, and unaltered oceanic basalts are represented by sediments from DSDP sites 294/295 (Vervoort et al., 2011), samples from the Bay of Islands ophiolite (Parendo et al., 2017), and the average E-MORB (Gale et al., 2013), respectively. The Nd isotopic ratio of clay-rich sediments is 0.512380 (Vervoort et al., 2011), whereas the Nd isotopic compositions of highly altered oceanic crust and unaltered oceanic basalts are assumed to be similar to that of the average E-MORB (0.513074) (Gale et al., 2013). The Th/U and Ba/Th ratios of these components are 6.64 and 35 (Vervoort et al., 2011), 2.5 and 166 (Parendo et al., 2017), and 3.54 and 92 (Gale et al., 2013), respectively.